Appl. Phys. B 66, 417–426 (1998)

Applied Physics B
Lasers
and Optics

High efficiency discharge-pumped XeCl laser

M. Makarov*, **J. Bonnet, D. Pigache**

ONERA, BP 72, 92322 Chatillon Cedex, France
(Fax: +33-01/6993-6182, E-mail: pigache@onera.fr)

Received: 19 March 1997/Revised version: 7 August 1997

Abstract. An X-ray preionized 0.7 l active volume discharge-pumped XeCl laser is described. A simple CLC resonant charging pumping scheme has been used. A specific laser energy of about 5 J/l at the efficiency of $> 5.5\%$ with respect to the electrical energy stored in the driving capacitors has been reached. A standard deviation $\sigma < 0.2\%$ was obtained for 3 J output energy.

PACS: 42.55; 42.60; 52.80

Until recently it was widely believed that good TEA laser performance requires an initial voltage as high as possible and applied in a very short time. Physically, this requirement was explained by the need for the uniform discharge formation [1, 2]. Thus, for the Ne-based XeCl laser, it was generally agreed that a $\sim 10^{-8}$ s voltage pulse of a minimum 2–3 kV/(cm bar) is necessary to achieve reasonable discharge quality [3–6].

However, the striving to increase the initial voltage across the gap inevitably came into conflict with the load matching condition. Since the basic requirement for efficient power transfer into a discharge from any LC energy store is $U_0 = 2U_{ss}$, where U_0 is the initial charging voltage and U_{ss} is the steady-state plasma voltage ($\simeq 0.5$ kV/(cm bar) for Ne/Xe/HCl mixtures), it seemed impossible to satisfy simultaneously both the gas breakdown condition and the voltage matching condition by using only one pumping circuit [6–8]. The double spiker-sustainer pumping method was introduced [8–15]. A comparison with other excitation techniques has shown the superior properties of the spiker-sustained excitation [11, 13, 15, 16].

It will be demonstrated that to attain a very high excimer laser performance

- there is no need to apply an excessively high initial voltage to the discharge gap,
- there is no need to do it so quickly,
- there is no need to use a double pumping circuit for perfect impedance matching.

The simplest CLC resonant charging pumping scheme was used. The discharge driving capacitors C_{dr} connected directly to the electrodes were pulse charged in a relatively long time of ~ 0.6–0.8 μs. A specific laser energy of about 5 J/l and an efficiency in excess of 5.5% (with respect to the electrical energy stored in C_{dr}) were reached at an initial voltage of only 1.1 kV/(cm bar).

1 Background reasoning

1.1 Streamer model of excimer discharge contraction

The short voltage rise time requirement was originally deduced by Levatter and Lin in 1980 [2] in addition to the minimum preionization electron density requirement postulated previously by Palmer [1] for the TEA discharges. The reasoning behind the model proposed is as follows.

A real high-pressure gas discharge is always driven by an electrical circuit of finite voltage rise time. If the initial voltage $U(t)$ across the discharge gap remains below the breakdown threshold U_{brd} for a non-zero period of time t_0 (pre-breakdown phase), then a spatial region of depth

$$x_0 = \int_0^{t_0} u_e(t)\ \mathrm{d}t = \int_0^{t_0} \mu E(t)\ \mathrm{d}t \propto \int_0^{t_0} U(t)\ \mathrm{d}t \qquad (1)$$

lacking free electrons will grow near the cathode. Here $u_e(t)$ and μ are the electron drift velocity and the electron mobility, $E(t)$ is the plasma electric field. In this case, the head of any noise electron avalanche within the depleted region x_0 will be separated from those of the nearest preionization electron avalanche by a streamwise distance of the order of x_0. Thus, to avoid undesirable streamer formation due to inadequate overlapping of the avalanches, it is necessary to keep

$$x_0 < r_c\,, \qquad (2)$$

* *On leave from*: High Current Electronics Institute, 4 Akademitcheski ave. 634055 Tomsk-55, Russia. Present address: SOPRA, 26 rue Pierre Joigneaux, F 92270 Bois-Colombes, France

where r_c is the so-called critical avalanche head radius. Since $r_c \propto t^{1/2}$ (free diffusion) depends on time to a smaller extent than $x_0 \propto t$ (electron drift), there is a definite threshold for the pre-breakdown phase duration t_{crit} above which inequality (2) is violated. In practice, the voltage rise time t_U is determined by the circuit configuration and hence is fixed. Thus, the simplest way to reduced t_0 is to build up the maximum voltage across the gap U_{max}

$$t_0 \sim t_U \frac{U_{brd}}{U_{max}} . \quad (3)$$

These speculations fitted in well with experience gathered with TEA N_2, CO_2, HF/DF lasers. It is hardly surprising that the great majority of subsequent investigations were carried out on this scheme (upper block of Table 1).

The "magic" of the high overvoltage was so strong that even new pumping concepts [9, 19, 20] were originally based on this requirement (lower block of Table 1). However, there was good reason to doubt the validity of the Levatter & Lin model.

1.2 Experimental contradiction with the streamer model

It was shown as early as 1980 by Taylor et al. [21] that even a very strong but *local* deterioration of the excimer discharge has little influence on the rest of the discharge. In remarkable experiments on laser preionization [10], one or another part of the discharge volume of a 100-ns XeCl laser was masked to prevent the production of the initial electrons. Complex-shaped masks were used. The burn patterns obtained on UV-sensitive paper faithfully copied the mask configuration. Notice that even though the laser output was drastically reduced in the masked regions, the laser energy over non-masked discharge remained essentially unchanged. In other words, *the* XeCl *discharge is hardly affected by the localized streamers and could be uniformly formed even with a non-uniform preionization.* If so, the requirement (2) seems not to be imperative.

Let us consider the case when an average preionization electron density is sufficiently high (experimental threshold level $N_{e0}^{min} \sim 10^8$–$10^9\,cm^{-3}$ [10, 22]) to provide a uniform discharge initiation.

It was observed experimentally that at the beginning of the pumping pulse, the uniform XeCl discharge is always formed *independently* of the initial voltage U_0 and its rise time t_U. As the discharge current increases up to $j/p \geq 10\,A/(cm^2\,bar)$, local plasma disturbances ("prespot") occur in the near-cathode zone depending on the electrode material and the surface conditions [23–25, 41]. Then, the high-current channel resting on the emission center ("hotspot") starts to grow towards the anode. The time interval between the prespot initiation and the channel formation is only about a few nanoseconds. When the high-current channel enters the homogeneous bulk, its further propagation across the discharge gap slows down. The higher the discharge current, the less the bulk plasma is affected by local instabilities. The experiments demonstrate that the surface density of hotspots drastically increases with increasing the $\partial j/\partial t$ parameter [25, 26]. Thus, the shorter the current rise time t_I, the higher the hotspots surface density and consequently, the higher is the discharge homogeneity.

Thus, it appears from the above discussion that:

- there is no physical limit to the initial discharge voltage except $U_0 > U_{brd}$;
- it is the current rise time t_I, not the voltage rise time t_U, that is of prime importance as far as the discharge uniformity is concerned.

1.3 Preliminary conclusions

The case in hand is the discharge-pumped Ne-based XeCl laser.

1. Because the steady-state reduced electric field is $(E/p)_{ss} \simeq 0.5$–$0.7\,kV/(cm\,bar)$, whereas the dc breakdown field is $(E/p)_{brd} \simeq 1\,kV/(cm\,bar) < 2(E/p)_{ss}$, the voltage matching between power supply and discharge load should present no problem.
2. Because the current rise time t_I depends on the discharge driving circuit inductance L, the most compact pumping scheme must be chosen. Use of the phototriggering technique seems promising [20, 27–30].
3. To create a homogeneous discharge, a strong gas preionization is needed. Recently designed X-ray preionizers easily reach the required initial level of $\sim (10^8 - 10^9)cm^{-3}$ in discharge volumes of any size [22, 31–35].

Thus, all the conditions for a uniform and efficient XeCl discharge formation could be met.

Table 1. Early stage of the discharge-pumped XeCl laser development (U_0 is the initial discharge voltage, U_{ss} is the steady-state discharge voltage, t_U is the voltage rise-time, e_{out} is the specific laser energy, η is the laser efficiency)

References		U_0/U_{ss}	t_U/ns	e_{out}/J/l	η (%)
[3]	(1981)	16	25	5.0	0.7
[4]	(1981)	13	25	3.2	—
[5]	(1982)	11	10	4.5	0.9
[6]	(1983)	9	10	5.0	1.4
[17]	(1984)	4 – 6	50	3.5	1.0
[18]	(1987)	9 – 13	50	4.4	1.0
[16]	(1988)	5 – 6	20	1.1	0.8
[9]	(1983)	6 *	20	3.5	4.2
[19]	(1986)	4 *	50	3.3	4.0
[20]	(1987)	5**	—	1.2	1.7

* spiker
** phototriggering

2 Experimental setup

In experiments the Deneb XeCl laser [22, 36–38] has been used as a test bed. Thus, it is the geometry of the laser chamber at our disposal that determines all the other laser parameters.

In this section we estimate first the chamber inductance to know the potential of the present setup. Second, the laser pumping conditions we need to achieve are calculated. Third, the discharge driving circuit designed according to the requirements is described. Then, the other laser subsystems are presented in detail.

2.1 Discharge chamber

The laser chamber and the two discharge electrodes are made of Ni-coated aluminum. The total chamber volume is about 10 l. The flat central part of the cathode is about 40 cm × 3 cm and the interelectrode gap is 5.3 cm. Thus, the active discharge volume is ∼ 0.6–0.7 l. The cathode edges were experimentally rounded to smooth the peripheral electric field.

The high-voltage electrode is mounted on a teflon insulator. A 2-cm-thick, glass-fiber-strengthened epoxy plate is used to close the chamber operated at a pressure of up to 6 bar (Fig. 1).

Following Champagne et al. [39] one can estimate the chamber inductance:

$$L_{\text{chamber}} \simeq \mu_0 \frac{d(h+6x)}{12 l_d} \simeq 4\pi \frac{dh}{l_d} (nH) \,, \tag{4}$$

where $\mu_0 = 4\pi \times 10^{-9}$ H/cm, d and h are the discharge gap and the discharge width respectively, and $x \simeq 2h$ is the distance between the edge of the discharge and the current returns. For $d = 5.3$ cm, $h = 3$–4 cm, and $l_d = 40$ cm, we obtain $L_{\text{chamber}} \simeq 5$–$6$ nH. This result agrees closely with those calculated from more precise analytic formulae [42] or obtained by computation [43]. Assuming the total driving inductance ($L = L_{\text{chamber}} + L_{\text{circuit}}$) to be about three times higher [28, 39], we estimate $L \approx 15$–18 nH as a lower limit for the present experimental setup.

2.2 Optimal pumping conditions

Using the XeCl laser optimization algorithm [28, 40], let us find the optimal discharge pumping conditions.

The pumping pulse duration is given by

$$t_{\text{pump}} \simeq \frac{\pi}{2} \frac{(e/p)_{\text{opt}}}{(j/p)_{\max} (E/p)_{\text{ss}}} \frac{1}{p} \simeq \frac{800}{p} \,, \tag{5}$$

where t_{pump} is in ns and p in bar. $(j/p)_{\max} \simeq 75$ A/(cm^2 bar) and $(e/p)_{\text{opt}} \simeq 0.025$ J/(cm^3 bar) are the maximum discharge current density and the specific energy deposition which should be reached for efficient XeCl laser pumping. For a total pressure of 5 bar, we have $t_{\text{pump}} \simeq 160$ ns.

By definition, for RLC electrical circuits, the peak current is

$$I_{\max} = \frac{U_0}{\rho + R} \,, \tag{6}$$

where U_0 is the initial store voltage, ρ and R are the power supply impedance and the load resistance respectively. In our case, $R = U_{\text{ss}}/I_{\max}$. Thus, from (6) we have for the circuit impedance

$$\rho = \frac{U_0 - U_{\text{ss}}}{I_{\max}} = \frac{U_{\text{ss}}}{I_{\max}} (k-1) \,, \tag{7}$$

where $k = U_0/U_{\text{ss}}$ is the overvoltage coefficient. It has been shown above that $k = 2$ can really be obtained. On the other hand, $\rho = \sqrt{L/C}$. Thus, the driving capacitance C and the inductance L are given by the simple expressions:

$$C \simeq \frac{1}{\pi} \frac{t_{\text{pump}}}{\rho} = \frac{1}{2} \frac{(e/p)_{\text{opt}}}{(E/p)^2_{\text{ss}}} \frac{h l_d}{d(k-1)} \frac{1}{p} \,, \tag{8}$$

$$L \simeq \frac{1}{\pi} t_{\text{pump}} \rho = \frac{1}{2} \frac{(e/p)_{\text{opt}}}{(j/p)^2_{\max}} \frac{d(k-1)}{h l_d} \frac{1}{p} \,, \tag{9}$$

where d, h, and l_d are the discharge height, width, and length respectively. The pulse duration $t_{\text{pump}} \simeq \pi\sqrt{LC}$ is taken into account in (8) and (9). For $d = 5.3$ cm, $h = 3$–4 cm, and $l_d = 40$ cm, we have $C \simeq 110$–130 nF and $L \simeq 15$–18 nH. Comparing this estimate of L (*"optimal circuit inductance"*) with that obtained above, it can be concluded that it is well within the permissible limits.

2.3 Driving circuit

The phototriggering pumping technique was used (Fig. 2). The energy store $C_1 = 123$ nF, made up of 42 ceramic capacitors UHV 2.7/30 (TDK), is connected directly to the discharge electrodes. The store is charged in ∼ 0.6–0.8 μs from the primary capacitor $C_0 = 229$ nF (Maxwell-31.160) through ∼ 2 m-length of coaxial high-voltage cable. The thyratron LS-4101 (EG&G) is used as a switch. No optimization has been made in the present study for the primary charge circuit. But it was verified that the efficiency of the $C_0 \longrightarrow C_1$ energy transmission can be sufficiently high, $> 75\% - 80\%$.

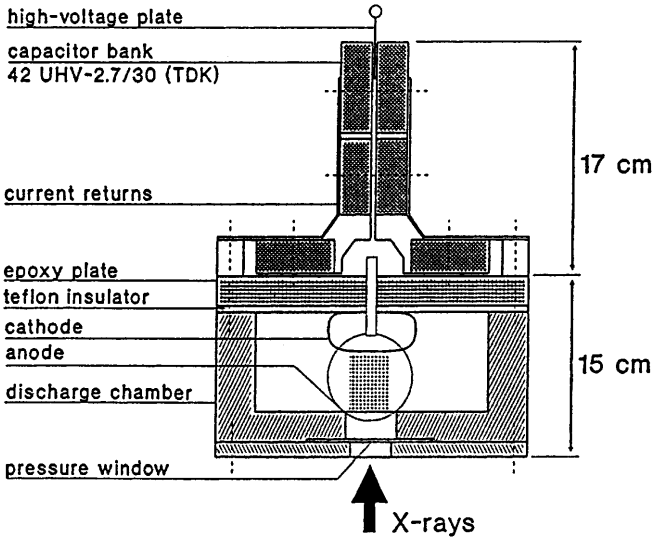

Fig. 1. Schematic drawing of the laser head

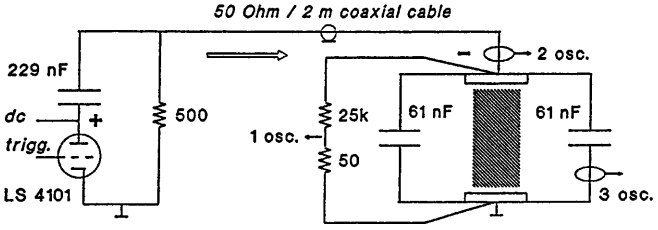

Fig. 2. Electrical pumping scheme. Primary capacitor $C_0 = 229$ nF; driving capacitors $C_1 = 123$ nF. Signal measurements: "1 osc." discharge voltage divider; "2 osc." discharge current home-made transformer; "3 osc." charge current Pearson transformer

2.4 Gas preionization

2.4.1 Preionization concept. The gas preionization is the central problem as far as the phototriggering discharge excitation is concerned [20, 25, 26, 35]. Because of the earlier high initial voltage requirement mentioned, it was previously concluded that, to be efficient, the preionization *must* be produced by a pulse of very short duration (~ 10 ns) [20, 35]. But an uncontrolled discharge breakdown due to parasitic electric charges led to a modification of the concept. The initial voltage was reduced, resulting clearly in a drastic increase of the discharge efficiency. The discharge driving capacitors had to be charged faster than previously (< 400 ns instead of 10 μs), and the preionization time was shifted to the voltage pulse beginning [29, 30].

As demonstrated earlier [27, 28, 38], high XeCl laser performance is quite possible using a long pulse preionizer. A low initial discharge voltage ($\leq 3U_{ss}$) was chosen from the beginning. It was shown that, in this case, the effective preionization time could be increased up to 100–200 ns [25]. Thus, there is no need to use a fast preionization. X-ray guns with ~ 200 ns rise time were successfully employed. A similar technique is utilized in the present study.

2.4.2 Preionizer design. The X-ray generator consists of a secondary emission electron gun as described previously [22].

The electron gun is composed of a pulsed helium ion source ($p \simeq 30$ μbar). The high-voltage cathode is polarized up to -120 kV by a pulse transformer. A gold-coated aluminium output window is used. The X-ray pulse time variation is measured with a plastic scintillator connected by an optical fiber to a photomultiplier. Typical waveforms are presented in Fig. 3 The X-ray pulse duration is about 400 ns (FWHM).

The X-rays pass through a 1-mm-thick pressure window and a 0.6 mm thick anode, both made of 25 μm Ni-coated aluminum.

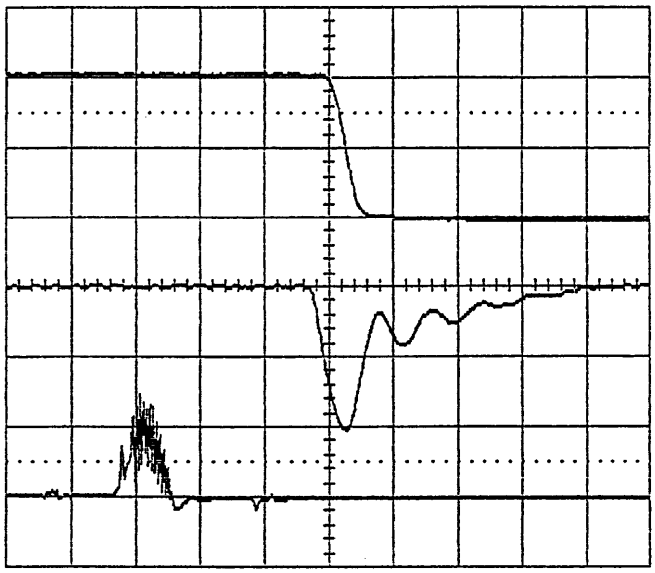

Fig. 3. X-ray preionizer operating conditions. The traces from the bottom: the ion source current, 100 A/div; the cathode voltage, 60 kV/div; the X-ray dose. Time scale is 1 μs/div

The integrated X-ray dose in air, measured with a pen dosimeter in the discharge gap, reaches ~ 18 mrad/pulse in the anode plane and ~ 10 mrad/pulse in the cathode plane. The preionisation uniformity in a plane perpendicular to the electric field was measured with Kodak Industrex AX film. The results are shown in Fig. 4 Particular attention was given to the pulse-to-pulse X-ray dose stability. The dose profiles accumulated over series of about 10^3 shots are shown in Fig. 5 (external triggering) For the optimized operating regime, the standard deviation $\sigma \sim 10\%$ was obtained for the dose integrated over the first ~ 200 ns of the X-ray pulse – the duration of interest as far as the low initial voltage, $(E/p)_0 \simeq$ 1–1.5 kV/(cm bar), phototriggered discharge is concerned.

2.5 Subsystem synchronization

The synchronization of the ion source, the electron gun driving circuit, and the discharge pumping network is handled by an optical fiber communication system for EMI protection. The optimal time delays were experimentally adjusted for the best laser output parameters (laser energy and its pulse-to-pulse stability).

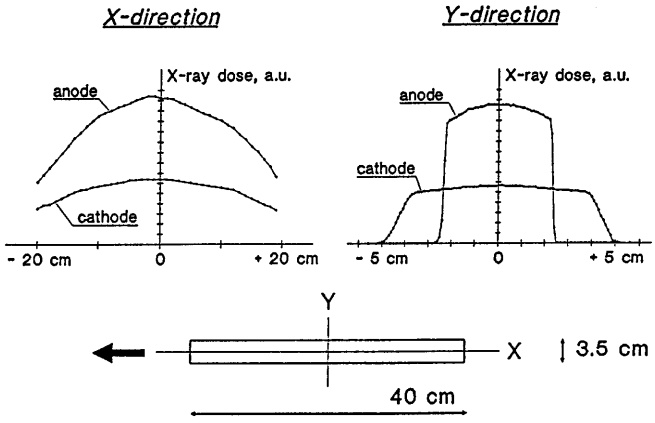

Fig. 4. Preionization uniformity. The *X* direction is the laser axis

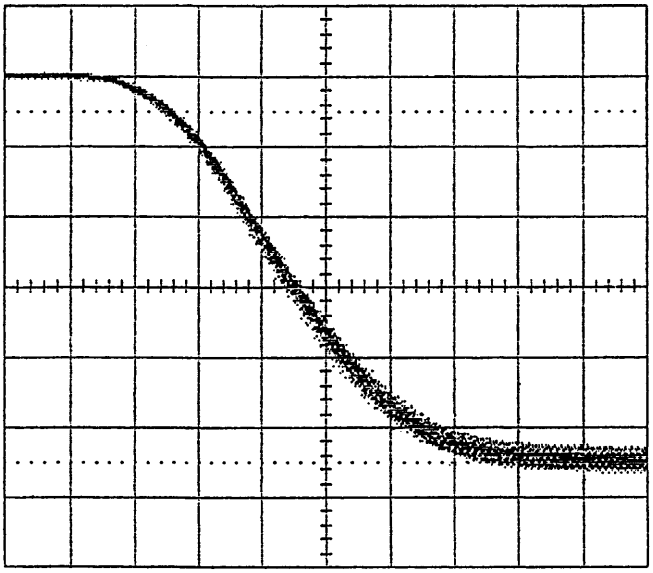

Fig. 5. X-ray dose $D(t)$ stability (10^3 pulses). Time scale is 100 ns/div

Typical waveforms of discharge voltage $U_d(t)$, discharge current $I_d(t)$, charge current $I_0(t)$, and X-ray dose $D(t)$ are shown in Fig. 6 (current oscillations at the pulse beginning are due to the electric wave back reflection because of imperfection of the $C_0 \rightarrow C_{cable} \rightarrow C_1 = \Sigma C_i$ circuit matching). The synchronization between $U_d(t)$ and $D(t)$ was retained throughout the experiment. A jitter of about 10 ns was found to have no influence on the laser performance.

2.6 Optical cavity configuration

A 72-cm-base plano/plano optical resonator is used. It is directly mounted on the discharge chamber. Two total reflectors, a $\sim 92\%$ reflection aluminum coated mirror or a $\sim 99\%$ multi-layer dielectric coated mirror, as well as two output couplers, a $\sim 8\%$ uncoated fused silica plate and a $\sim 23\%$ one-side-treated one, were tested.

2.7 Measurements

The discharge current is measured by a home-made current transformer embracing one of the two current returns ("3 osc." in Fig. 2). The voltage across the driving capacitor bank C_1 (hereafter referred to as the discharge voltage) is measured by a carbon resistor voltage divider (24.988 kΩ/49.6 Ω) connected to an oscilloscope through a 50 Ω coaxial cable ("1 osc." in Fig. 2). Both probes were carefully calibrated with a known LC oscillator circuit using the Pearson-110A standard current monitor and a stabilized dc high-voltage generator.

The laser output energy is measured by a disc calorimeter 38-0402 (Scientech). The expected laser power density of about 30 MW/cm^2 is much higher than the damage threshold of the working surface coating, so the calorimeter has been modified. A 2-mm single-side polished optical glass plate was stuck on to the calorimeter disc with a heat-conducting grease. The glass type was specially chosen for the penetration depth of 308 nm laser radiation to be approximately equal to the plate thickness. Then, the calorimeter was recalibrated for the 5 J range according to the operating instructions. A 4% beam reflection from the front side of the glass plate was taken into account.

A pyroelectric joulemeter ED-500 (Gentec) is used for the laser energy pulse-to-pulse stability measurement.

The laser-pulse profile is measured in the following way. To be well mixed, the $\sim 2.5\,\text{cm} \times 5\,\text{cm}$ cross-section laser beam is focussed on a matt silica plate positioned 50 cm from a $F = 30$ cm quartz lens. The scattered UV radiation is collected and transferred to a photodiode by a silica optical fiber. The position of the fiber entrance is chosen for the optical signal to be under the diode saturation level.

A four-channel 200 MHz digital oscilloscope Lecroy 9304A is used for electric signals measurements.

The gas pressure is controlled by a 1–5 bar MKS 310BJS-10 (Baratron) system. Neon N40 and xenon from Alphagaz (L'air liquide) and HCl from Messer Griesheim are used as active mixture components. A gas purifier, GP2000XR (Oxford Lasers Ltd), operating at 140 K is used.

2.8 Operating conditions

The laser pumping parameters are summarized in Table 2.

3 Experimental results and discussion

3.1 Electrical characteristics

Typical signal waveforms are presented in Fig. 7. To analyze the pumping process, let us consider its fundamental stages.

In general, the discharge voltage $U_d(t)$ has no time to flatten, then a non-zero and negative charge current $I_0(t)$ flows before the breakdown (Fig. 8). A detectable discharge current in the opposite direction appears at the breakdown instant 1. However, the voltage drop occurs somewhat later, at the instant 2, when the discharge current I_d exceeds the charge current I_0.

It should be noted that towards the end of the pre-breakdown phase 1–2, the discharge is already formed with

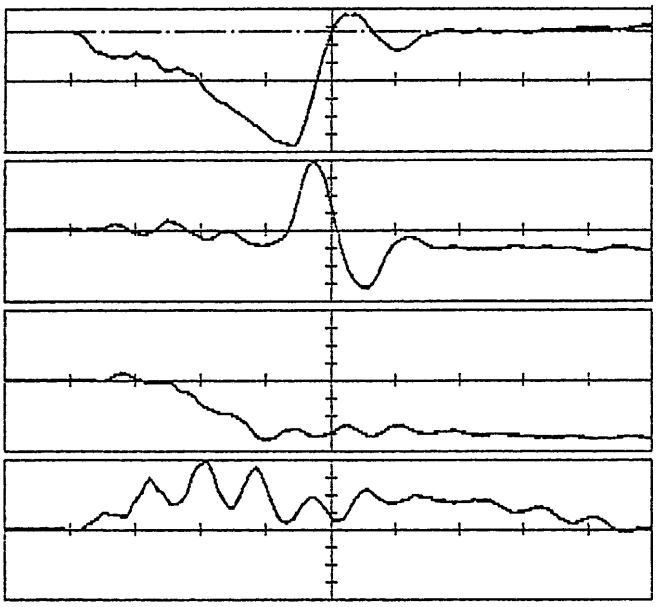

Fig. 6. Typical waveforms of the charge current, the X-ray dose, the discharge current, and the discharge voltage (from the bottom, in arbitrary units). Time scale is 200 ns/div

Table 2. Pumping parameters of the modified Deneb XeCl laser

Parameter	
discharge volume, cm^3	$5.3 \times (2.5 - 3.5) \times 40$
total gas pressure, bar	$3 - 5$
mixture composition, Ne/Xe/HCl	1000/8/0.8
X-ray pulse duration, ns	400 (FWHM)
X-ray dose, mrad/pulse	$10 - 18$
primary store capacitance, nF	229
initial voltage, kV	up to 35
charge current, kA	up to 10
charge pulse duration, ns	$700 - 800$
driving capacitance, nF	123
initial discharge voltage, kV	up to 33
maximum discharge current, kA	up to 40
pumping pulse duration, ns	150

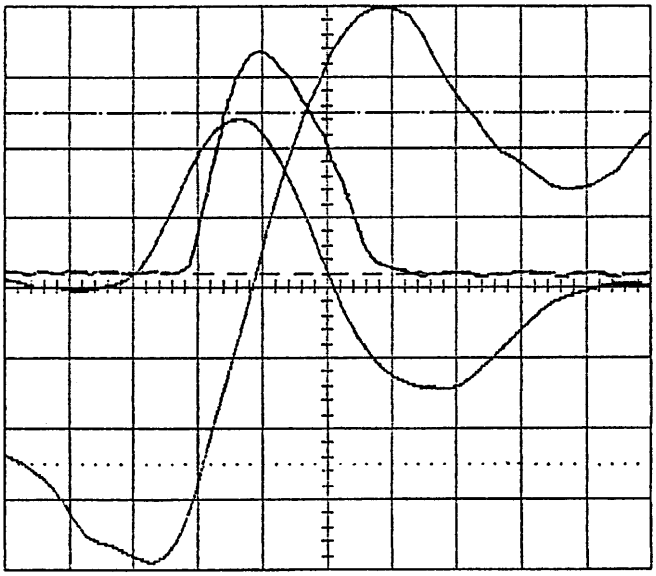

Fig. 7. Typical waveforms of the discharge voltage (5 kV/div, $U_d = 0$ is marked by $-\cdot-$), the discharge current (15 kA/div, $I_d = 0$ is marked by $---$), and the laser pulse. Ne/Xe/HCl = 1000/8/0.8, $p = 5$ bar. Time scale is 50 ns/div

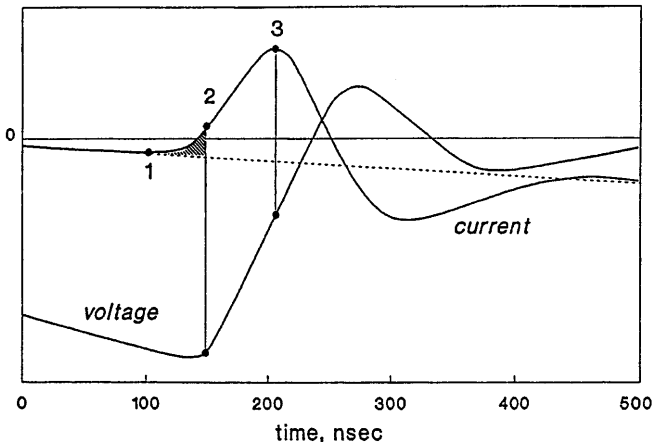

Fig. 8. Flow chart of the discharge pumping process. $1-2$ is the pre-breakdown phase

a current density of ~ 50 A/cm^2 and a plasma resistance of $\sim 1\,\Omega$. In other words, some energy is delivered before the voltage drop. We can estimate this additional energy ΔE_{in} deposited into the discharge *directly from the primary circuit*. For ~ 5 kA charge current and ~ 30 kV initial discharge voltage, the energy transferred to the plasma during the ~ 30 ns pre-breakdown phase 1–2 is ~ 5 J. So, despite the fact that the primary circuit inductance (800 nH) is much higher than the discharge circuit inductance (18 nH), the correction ΔE_{in} must be taken into account when evaluating the laser efficiency [30].

After the breakdown 2, the discharge rapidly achieves a steady state where the plasma voltage remains nearly constant, $U_{\text{pl}} \simeq (E/p)_{\text{ss}}\, pd$. The duration of this stage depends on the power deposition and the discharge uniformity and in principle can proceed up to the end of the pumping pulse. The steady state electric field $(E/p)_{\text{ss}}$ could be easily deduced from the experimental discharge voltage at the instant

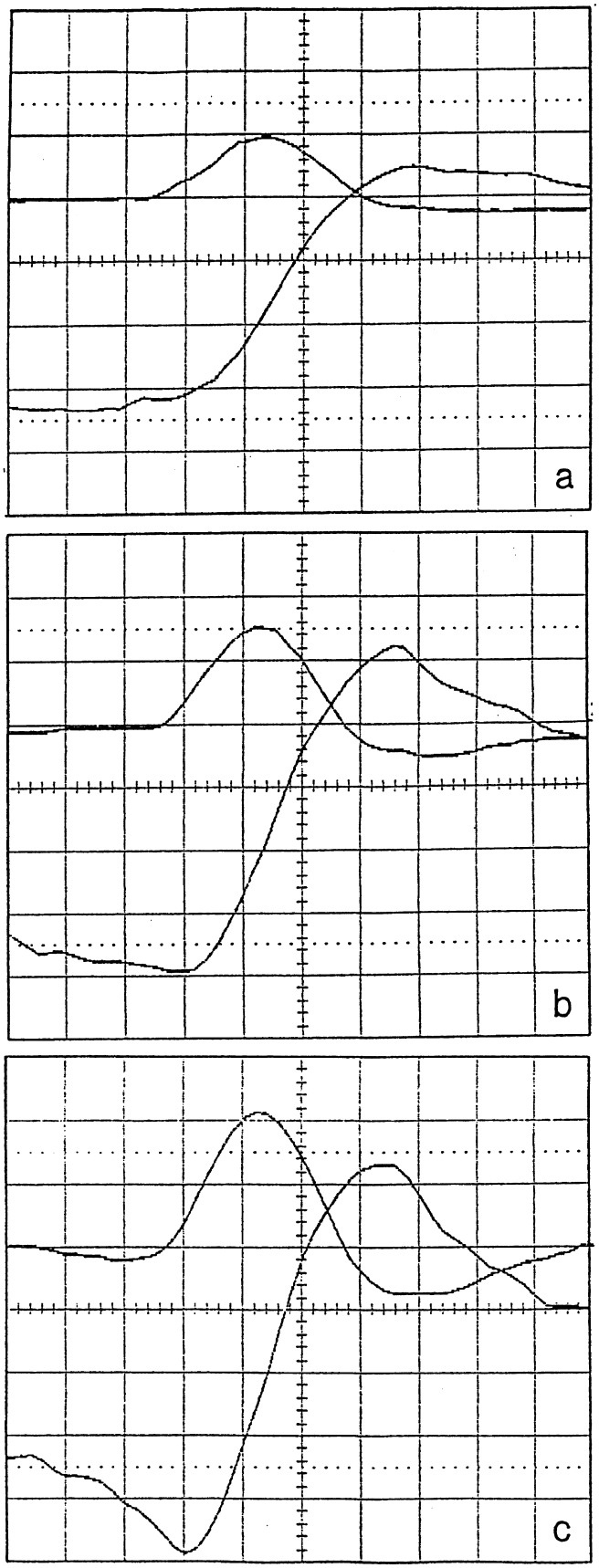

Fig. 9a–c. Typical waveforms of the discharge voltage (5 kV/div), the discharge current (15 kA/div) taken upon a gradual increase of U_0 at $p = 3$ bar. The overvoltage coefficient: **a** $k = 1.6$, **b** $k = 1.85$, **c** $k = 2.25$. Time scale is 50 ns/div

3 when the discharge current is a maximum I_{max}, as the inductive correction $\Delta U = L_{chamber} \times \partial I/\partial t = 0$. The evolution I_{max} versus initial voltage U_0 across the gap was experimentally found to be linear, as predicted by (6). The value $(E/p)_{ss} \simeq 0.65$–0.70 kV/(cm bar) is obtained; it is independent of the total gas pressure.

As noted earlier, for RLC circuits, current oscillations inevitably take place. The extent to which oscillations are pronounced depends on the ratio R/ρ. Assuming the discharge to be uniform during all the pumping pulse, i.e. the discharge filamentation did not take place and the plasma resistance depends only on the volume-average current, one can write:

$$R(t) = \frac{U_{pl}(t)}{I_d(t)} \sim \frac{U_{ss}}{I_{max}} . \quad (10)$$

Using (7), we have from (9)

$$\frac{R_d}{\rho} \sim \frac{1}{k-1} , \quad \text{where} \quad k = \frac{U_0}{U_{ss}} = \frac{U_0}{(E/p)_{ss} pd} \propto \frac{U_0}{p} . \quad (11)$$

It is seen from (11) that an increase in the initial voltage U_0 and a decrease in the total gas pressure p lead to an impedance dismatching in the same manner. Experimental $U_d(t)$ and $I_d(t)$ waveforms taken upon a gradual increase of U_0 at $p = 3$ bar are shown in Fig. 9 Very similar results have been obtained for other values of p.

3.2 Laser energy

The laser energy E_{out} versus the initial discharge voltage U_0 is presented in Fig. 10a. A maximum value of about 3.5 J/pulse has been obtained. It corresponds to a specific energy extraction of ~ 5 J/l. No saturation has been observed for the $E_{out}(p)$ dependence over 35 kV operating voltage limited by the TDK capacitors.

One can plot the laser energy E_{out} as a function of initial reduced electric field $(E/p)_0$. The results are shown in Fig. 10b. They tend to prove the idea, postulated before, that the XeCl laser can already operate well at $(E/p)_0 \sim 1$ kV/(cm bar), i.e. within the near vicinity of the breakdown threshold.

Different optical cavities were tested to optimize the resonator coupling (see Sect. 2.6). The dependencies obtained

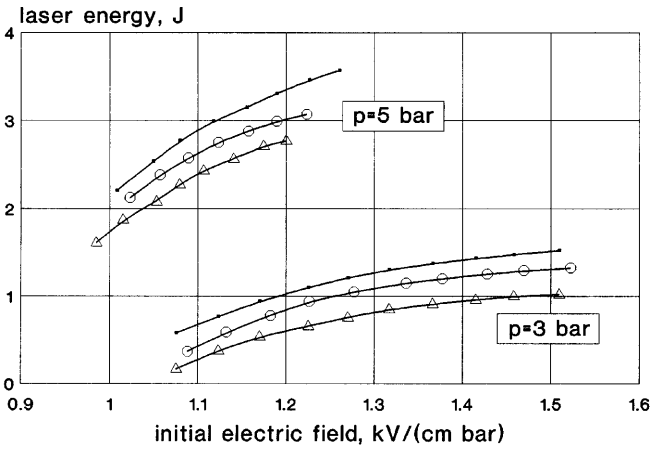

Fig. 11. Laser energy vs initial reduced electric field for different resonator configuration: • 99% reflection dielectric-coated mirror and 23% reflection output window; ○ 92% reflection aluminum-coated mirror and 23% reflection output window; △ 92% reflection aluminum-coated mirror and 8% reflection output window

(Fig. 11) demonstrate a similar behavior over all the ranges of U_0 and p. In our case, the resonator made of a multi-layer dielectric-coated total reflector and a 23% coupler, was found to be the best.

Moderate pumping power (i.e. moderate halogen donor depletion) and high discharge uniformity allow the laser pulse to proceed up to the end of the first half-period of the discharge-current pulse and even further (Fig. 7). With a 30% reflection coupler, the laser pulse tail lengthens considerably and its second maximum (or, more precisely, the plateau) appears, corresponding to the second half-period of the discharge current. This suggests that the laser pulse terminates not because of discharge filamentation, but merely because of a decline in pumping power.

3.3 Laser efficiency

As noted above, the $C_0 \rightarrow C_1$ charge circuit and the discharge pumping circuit are not independent before the voltage drop 2 (Fig. 8). However, the additional energy $\Delta E_{in} \sim 0.05 E_0$ deposited into the discharge during the pre-breakdown stage and coming from the primary circuit was found to be fairly

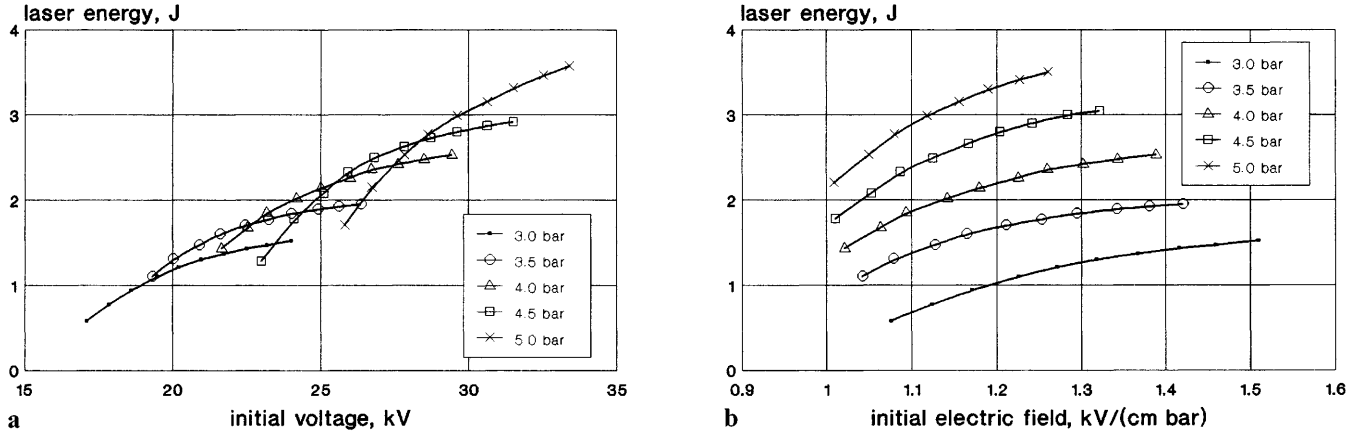

Fig. 10a,b. Laser energy vs **a** initial discharge voltage and **b** initial reduced electric field. The resonator: 99% reflection dielectric-coated mirror and 23% reflection output window

constant whatever the discharge conditions. A possible reason is that an increase in charge current (for example, due to a buildup of initial voltage across the primary capacitor C_0) causes the pre-breakdown phase to shorten; thus, the delivered energy changes slightly.

On the other hand, after breakdown 2 the discharge pumping is a truly independent process (Fig. 6) and thus it can be considered in its own right. Doing so, the laser efficiency η was calculated as the ratio of the output energy E_{out} to the energy stored in the driving capacitors $E_0 = C_1 U_0^2/2$, whereas the ΔE_{in} was taken into account as a correction.

The dependencies $\eta(U_0)$ and $\eta(E/p)$ are presented in Figs. 12 and 13 respectively. The best efficiencies $E_{\text{out}}/E_0 \sim 5.5\%$ and $E_{\text{out}}/(E_0 + \Delta E_{\text{in}}) > 5\%$ were obtained at $(E/p)_0 \simeq 2(E/p)_{\text{ss}}$ *independently* of gas pressure (Fig. 13b), as predicted for an ideal RLC circuit.

Really, the energy deposed in the plasma during the first half-period of the current pulse can be expressed

$$E_{\text{in}} = \int_0^{t_{\text{pump}}} I_{\text{d}}(t) U_{\text{pl}}(t)\, \mathrm{d}t \simeq \frac{2}{\pi} I_{\max} U_{\text{ss}} t_{\text{pump}} . \tag{12}$$

Using $t_{\text{pump}} = \pi\sqrt{LC} = \pi C\rho$, from (6) we obtain for the energy deposition

$$E_{\text{in}} \simeq 2\, C U_{\text{ss}}^2 \left(\frac{U_0}{U_{\text{ss}}} - 1\right) . \tag{13}$$

Then, the impedance-matching efficiency, $\eta' = E_{\text{in}}/E_0$, can be expressed

$$\eta' \sim \left(\frac{U_{\text{ss}}}{U_0}\right)^2 \left(\frac{U_0}{U_{\text{ss}}} - 1\right) = \frac{k-1}{k^2} . \tag{14}$$

As could be expected, (14) shows that the matching efficiency depends only on the initial overvoltage k. The similar dependence for $\eta = E_{\text{out}}/E_0$ observed experimentally is indicative of very high discharge uniformity.

3.4 Pulse-to-pulse laser stability

The laser energy pulse-to-pulse stability measurements were made for a continuous operating regime at 0.1 Hz using both a disc calorimeter and a pyroelectric joulemeter. The results were found to be very similar. In the first case, the signal is

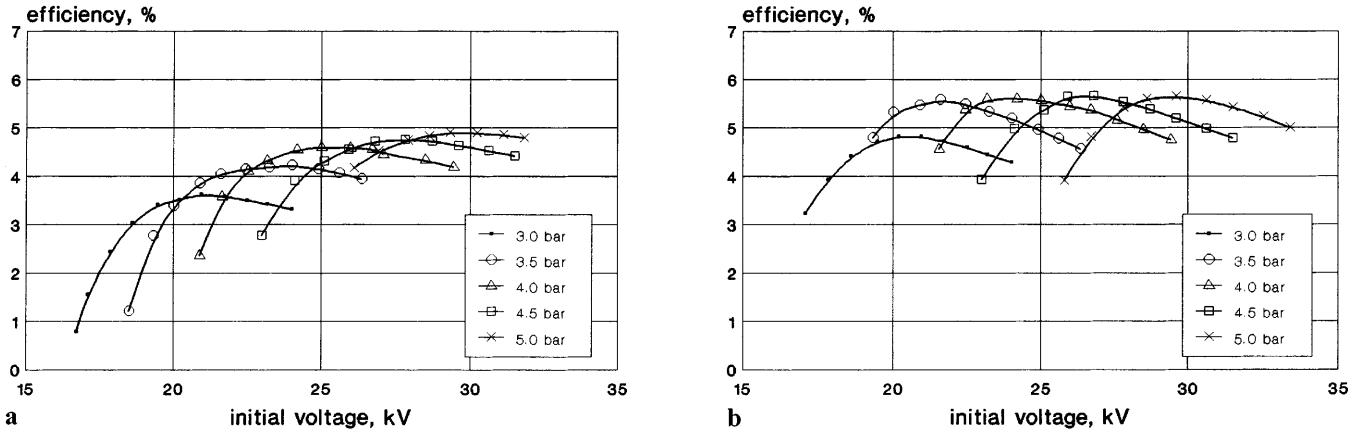

Fig. 12a,b. Laser efficiency E_{out}/E_0 vs initial discharge voltage for different resonators: **a** 92% reflection aluminum-coated mirror and 8% reflection output window; **b** 99% reflection dielectric-coated mirror and 23% reflection output window

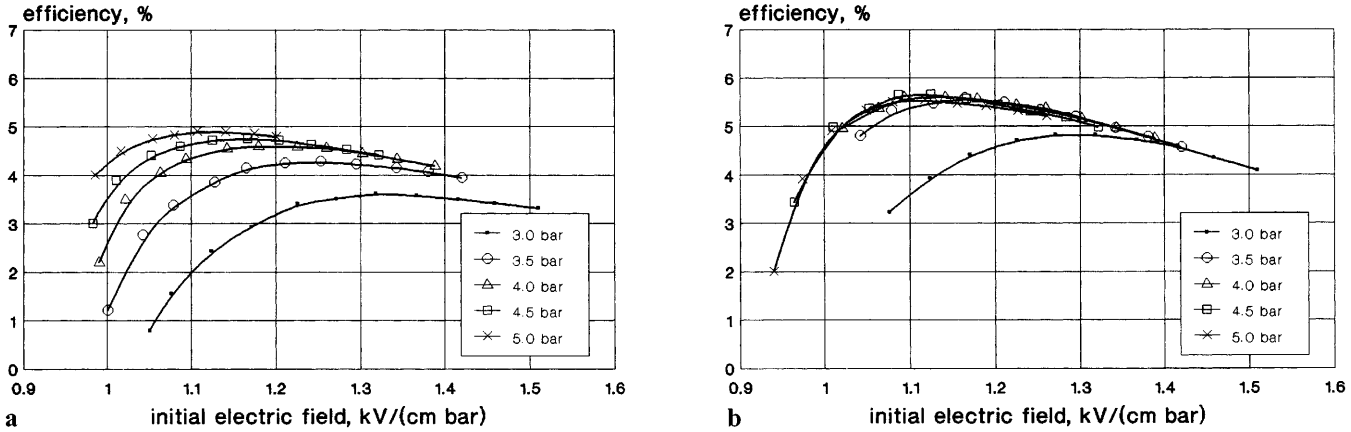

Fig. 13a,b. Laser efficiency E_{out}/E_0 vs initial reduced electric field for different resonators: **a** 92% reflection aluminum-coated mirror and 8% reflection output window; **b** 99% reflection dielectric-coated mirror and 23% reflection output window

recorded by a linear plotter and then processed. The diagrams obtained are presented in Fig. 14. To verify the sensitivity, the calorimeter was masked for a single laser shot resulting in a 100% signal variation (Fig. 14a).

In the second case, the signal is recorded by an oscilloscope and processed automatically.

The laser energy was found to be stabilized only after ~ 300 shots. This intermediate phase is probably due to (i) self-cleaning of the discharge electrodes, (ii) pyrolysis of uncontrolled impurities in the active gas mixture and establishment of a plasma-chemical balance, and (iii) thermostabilization of the gas purifier.

For a 3 J laser energy, the joulemeter output signal is 3 ± 0.005 V over one hour continuous operation at 0.1 Hz. It corresponds to a standard deviation $\sigma < 0.2\%$.

4 Conclusions

The pumping circuit design exerts a great influence on TEA laser performance. The basic parameter here is *the energy deposition* into the gas. It means not only the energy E_{in} deposited during the first half-period of the pumping pulse t_{pump}, but also the energy E'_{in} released during unavoidable afterpulse current oscillations. Usually, this energy does not contribute to laser output. On the contrary, it has a number of detrimental effects.

1. The voltage reversal is very undesirable as far as the lifetime of discharge driving capacitors and thyratrons is concerned.
2. An unutilized energy release during the final arc discharge phase stresses the discharge electrodes. First, it short-

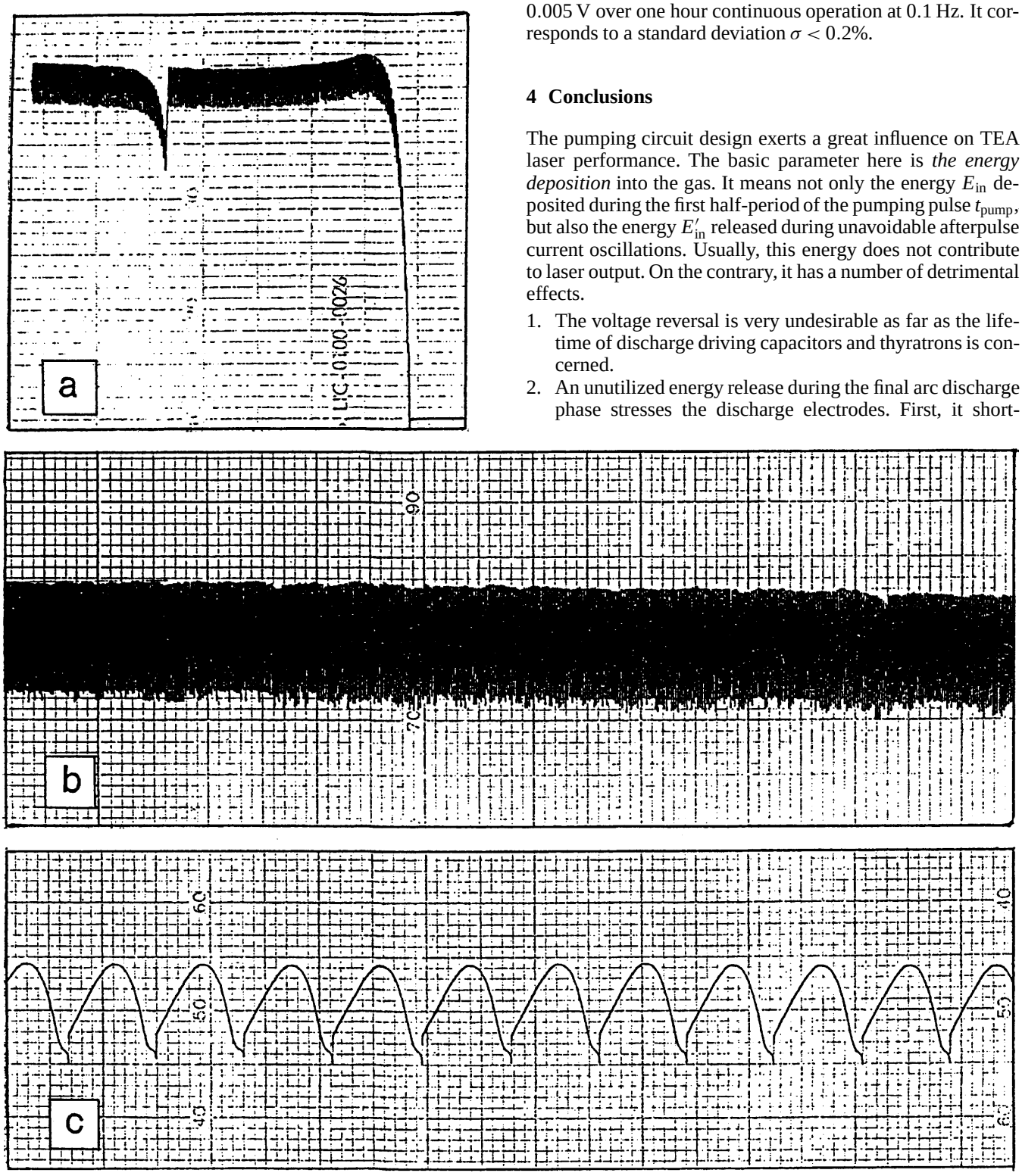

Fig. 14a–c. Laser energy measured by a disc calorimeter for 3.5 J/pulse, 0.1 Hz continuous operating regime. **a** intermediate phase (first 300 pulses). The signal drop is due to a single pulse masking. **b** and **c** stabilized phase (~ 700 pulses) for different plotter paper speeds

ens the electrode lifetime. Second, the degradation of the working surface leads to dust production from electrode sputtering.
3. The gas lifetime is shortened due to a strong depletion of the halogen donor during the arc afterpulse.
4. In many applications the high EMI level caused by the current oscillation cannot be ignored.
5. The pulse-to-pulse laser output instability is, primarily, due to the plasma instability, which is more pronounced in a filamented non-optimized discharge.

Thus the basic requirement for a high performance TEA laser is that the energy which remains in the discharge driving circuit after the laser pulse should be as small as possible. This regime has been realized in the present study.

The main results are the following:

- a $\sim 3.5\,\mathrm{J/pulse}(\sim 5\,\mathrm{J/l})$ discharge pumped XeCl laser is designed;
- a $< 0.2\%$ population standard deviation is obtained for 3 J output energy;
- a $\sim 5.5\%$ laser efficiency with respect to the electrical energy stored in the driving capacitors is reached;
- a 400-ns-long (FWHM) moderate-power X-ray pulse is used as a preionizer;
- a high laser performance is realized with an initial electric field of only about $1.1\,\mathrm{kV/(cm\,bar)}$ and a ~ 700–$800\,\mathrm{ns}$ discharge voltage rise time.

Taken together, these characteristics are believed to be the best ever reached with a XeCl laser.

These laser characteristics are very favorable for various applications:

1. the design of more compact and cheaper laser systems for industrial use is possible with efficient operation and no high-voltage/current switch in the discharge circuit;
2. a high laser-beam quality can be achieved with a discharge of very good uniformity, using either unstable cavities or seeder–amplifier methods;
3. a multi-joule laser output and a high pulse-to-pulse stability make possible, for example, gas or plasma single-shot probing and are also very convenient for material processing.

Acknowledgements. This work was supported in part by MENESRIP of France. The authors would like to thank Prof. Yuri Bychkov (HCEI, Tomsk, Russia) and Dr. Bruno Godard (SOPRA, Bois Colombes, France) for their helpful suggestions and discussions.

References

1. A.J. Palmer: Appl. Phys. Lett. **25**, 138 (1974)
2. J.I. Levatter, S.-C. Lin: J. Appl. Phys. **51**, 210 (1980)
3. S.-C. Lin, Z. Bao, G. Gong, Y. Huo, J. Shu, S. Tang, Y. Wei, C. Zheng: Appl. Phys. Lett. **38**, 328 (1981)
4. J.I. Levatter, K.L. Robertson, S.-C. Lin: Appl. Phys. Lett. **39**, 297 (1981)
5. H. Shields, A.J. Alcock: Opt. Commun. **42**, 128 (1982)
6. R.S. Taylor, P.B. Corkum, S. Watanabe, K.E. Leopold, A.J. Alcock: IEEE J. Quantum Electron. **QE-19**, 416 (1983)
7. M.R. Osborn, P.W. Smith, M.H.R. Hutchinson: Opt. Commun. **52**, 415 (1985)
8. R.S. Taylor, K.E. Leopold: Appl. Phys. Lett. **46**, 335 (1985)
9. W.H. Long, M.J. Plummer, E.A. Stappaerts: Appl. Phys. Lett. **43**, 735 (1983)
10. R.S. Taylor: Appl. Phys. B **41**, 1 (1986)
11. R.S. Taylor, K.E. Leopold: J. Appl. Phys. **65**, 22 (1989)
12. C.M. Timmermans, F.A. van Goor, W.J. Witteman: Appl. Phys. B **57**, 441 (1993)
13. F.A. van Goor, W.J. Witteman, C.M. Timmermans, J. van Spijker, J. Couperus: Proc. Intern. Conf. on High-Power Gas and Solid State Lasers SPIE **2206**, 30 (1994)
14. R.S. Taylor, K.E. Leopold: Appl. Phys. B **59**, 479 (1994)
15. N. Bernard, Th. Hofmann, B.L. Fontaine, Ph. Delaporte, M. Sentis, B.M. Forestier: Appl. Phys. B **62**, 431 (1996)
16. T. Letardi, S. Bollanti, P. Di Lazzaro, F. Flora, G. Giordano, T. Hermsen, C.E. Zheng: Proc. Intern. Cong. on Optical Science and Engeneering, Hamburg (1988)
17. L.F. Champagne, A.J. Dudas, B.L. Wexler: Proc. Intern. Conf. on Excimer Lasers and Applications SPIE **476**, 2 (1984)
18. T. Hasama, K. Miyazaki, K. Yamada, K. Ohuchi, T. Sato: J. Appl. Phys. **61**, 4691 (1987)
19. C.H. Fisher, M.J. Kushner, T.E. DeHart, J.P. McDaniel, R.A. Petr, J.J. Ewing: Appl. Phys. Lett. **48**, 1574 (1986)
20. B. Lacour, C. Vannier: J. Appl. Phys. **62**, 754 (1987)
21. R.S. Taylor, A.J. Alcock, K.E. Leopold: Opt. Lett. **5**, 216 (1980)
22. J. Bonnet, D. Pigache, E. Estocq, P. Laborde, M. Stehle: Proc. Int. Symp. on Gas Flow and Chemical Lasers SPIE **1031**, 374 (1988)
23. R. Dreiskemper, G. Schröder, W. Bötticher: IEEE Trans. Plasma Sci. **23**, 180 (1995)
24. R. Dreiskemper, W. Bötticher: IEEE Trans. Plasma Sci. **23**, 987 (1995)
25. M. Makarov: J. Phys. D: Appl. Phys. **28**, 1083 (1995)
26. M. Makarov, Yu. Bychkov: J. Phys. D: Appl. Phys. **29**, 350 (1996)
27. Yu. Bychkov, M. Makarov, M. Vinnik: Sov. J. Quantum Electr. **22**, 498 (1992)
28. Yu. Bychkov, M. Makarov, A. Suslov, A. Yastremsky: Rev. Sci. Instrum. **65**, 28 (1994)
29. B. Lacour, H. Brunet, H. Besaucele, C. Gagnol: Proc. Int. Conf. Gas Flow and Chemical Lasers SPIE **1810**, 368 (1992)
30. B. Lacour, H. Besaucele, H. Brunet, C. Gagnol, B. Vincent: Proc. Int. Conf. Gas Flow and Chemical Lasers, SPIE **3092**, 362 (1996)
31. D. Pigache, J. Bonnet, D. David: Proc. ICPIG XVI, Dusseldorf, 782 (1983)
32. T. Letardi, P. Di Lazzaro, G. Giordano, C.E. Zheng: Appl. Phys. B **48**, 55 (1989)
33. S. Bollanti, P. Di Lazzaro, F. Flora, G. Giordano, T. Letardi, G. Schina, C.E. Zheng: Rev. Sci. Instrum. **65**, 315 (1993)
34. F.A. van Goor: J. Appl. Phys. D **26**, 404 (1993)
35. R. Riva, M. Legentil, S. Pasquiers, V. Puech: J. Phys. D: Appl. Phys. **28**, 856 (1995)
36. B. Godard, E. Estocq, M. Stehle, P. Laborde, J. Bonnet, D. Pigache: Proc. Int. Conf. Excimer Lasers and Applications SPIE **1278**, 92 (1990)
37. B. Godard, E. Estocq, F. Joulain, P. Murer, M. Stehle, J. Bonnet, D. Pigache: Proc. Int. Conf. Excimer Lasers and Applications SPIE **1503**, 71 (1991)
38. J. Bonnet, D. Pigache, M. Makarov, B. Godard, M. Stehle,: Proc. Int. Conf. Gas Flow and Chemical Lasers SPIE **2502**, 421 (1994)
39. L.F. Champagne, A.J. Dudas, N.W. Harris: J. Appl. Phys. **62**, 1576 (1997)
40. M. Makarov: Rev. Sci. Instrum. **68**, 3975 (1997)
41. W. Bötticher, H. Lück, St. Niesner, and A. Schwabedissen: Appl. Phys. B **54**, 295 (1992)
42. F.W. Grover: *Inductance Calculations*, (D. van Nostrand Comp. Inc., New York 1947)
43. T. Letardi, F. Flora, C.E. Zheng: *Inductance Calculation of Discharge Chamber for Transversely Gas Flow Laser System*, (ENEA report RT/TIB/89/59, Frascati, Italy 1989)